Biological/Biomedical Accelerator Mass Spectrometry Targets. 2. Physical, Morphological, and Structural Characteristics

Seung-Hyun Kim,[†] Peter B. Kelly,[‡] and Andrew J. Clifford[†,]*

Department of Nutrition and Department of Chemistry, University of California Davis, One Shields Avenue, Davis, California 95616

The number of biological/biomedical applications that require AMS to achieve their goals is increasing, and so is the need for a better understanding of the physical, morphological, and structural traits of high quality of AMS targets. The metrics of quality included color, hardness/texture, and appearance (photo and SEM), along with FT-IR, Raman, and powder X-ray diffraction spectra that correlate positively with reliable and intense ion currents and accuracy, precision, and sensitivity of fraction modern (F_m). Our previous method produced AMS targets of gray-colored iron−carbon materials (ICM) 20% of the time and of graphite-coated iron (GCI) 80% of the time. The ICM was hard, its FT-IR spectra lacked the sp^2 bond, its Raman spectra had no detectable G′ band at 2700 cm^{-1}, and it had more iron carbide (Fe_3C) crystal than nanocrystalline graphite or graphitizable carbon (g-C). ICM produced low and variable ion current whereas the opposite was true for the graphitic GCI. Our optimized method produced AMS targets of graphite-coated iron powder (GCIP) 100% of the time. The GCIP shared some of the same properties as GCI in that both were black in color, both produced robust ion current consistently, their FT-IR spectra had the sp^2 bond, their Raman spectra had matching D, G, G′, D+G, and D″ bands, and their XRD spectra showed matching crystal size. GCIP was a powder that was easy to tamp into AMS target holders that also facilitated high throughput. We concluded that AMS targets of GCIP were a mix of graphitizable carbon and Fe_3C crystal, because none of their spectra, FT-IR, Raman, or XRD, matched exactly those of the graphite standard. Nevertheless, AMS targets of GCIP consistently produced the strong, reliable, and reproducible ion currents for high-throughput AMS analysis (270 targets per skilled analyst/day) along with accurate and precise F_m values.

Graphitization of solid carbon of biological/biomedical origin is a two-step process: first the carbon of a sample of interest is oxidized to CO_2, and second, the CO_2 is then reduced to graphitic materials. Graphite is a well-ordered crystal structure of carbon that is classified as natural or synthetic.[1,2] The H_2 or Zn reduction method has long been used for carbon dating and more recently for biological/biomedical AMS applications.[3−9] A variety of terms such as amorphous carbon (a-C),[10] graphite,[5] a fullerene "graphite",[6] or solid fullerene[11] have been used within and between prior reports to describe the material produced during the reduction of CO_2, CO, or both. While the physical, morphological, and structural characteristics of the AMS targets that had been produced seemed to vary within and between reports, they have not been studied systematically nor has the importance of their physical, morphological, and structural characteristics in maximizing ion current been well determined. Using Zn as the reductant, Jull et al.[12] first reported the formation of a mix of well-crystallized materials, poorly crystallized materials, and on occasion, a metal carbide (MeC). While nickel formed a different (more complicated) MeC compared to cobalt or iron,[4] MeC, in general, failed to produce a robust ion current so the ratios of $^{14}C/^{13}C$ varied by as much as 10% among replicate analyses.[5]

Therefore, in the present paper, we describe the color, hardness, texture, scanning electron microscopy (SEM), FT-IR transmission, Raman spectrometry, and XRD analyses of the accelerator mass spectrometry (AMS) targets (carbon material that coated over the −400 mesh spherical iron powder, −400MSIP) as prepared by our previous[7] and optimized[13] methods. Our goal

(1) Oya, A.; Marsh, H. *J. Mater. Sci.* **1982**, *17*, 309–322.

(2) Wissler, M. *J. Power Sources* **2006**, *156*, 142–150.

(3) Vogel, J. S.; Southon, J. R.; Nelson, D. E.; Brown, T. A. *Nucl. Instrum. Methods Phys. Res., Sect. B* **1984**, *5*, 289–293.

(4) Vogel, J. S.; Southon, J. R.; Nelson, D. E. *Nucl. Instrum. Methods Phys. Res., Sect. B* **1987**, *29*, 50–56.

(5) Vogel, J. S. *Radiocarbon* **1992**, *34*, 344–350.

(6) Ognibene, T. J.; Bench, G.; Vogel, J. S.; Peaslee, G. F.; Murov, S. *Anal. Chem.* **2003**, *75*, 2192–2196.

(7) Getachew, G.; Kim, S. H.; Burri, B. J.; Kelly, P. B.; Haack, K. W.; Ognibene, T. J.; Buchholz, B. A.; Vogel, J. S.; Modrow, J.; Clifford, A. J. *Radiocarbon* **2006**, *48*, 325–336.

(8) Lin, Y.; Dueker, S. R.; Follett, J. R.; Fadel, J. G.; Arjomand, A.; Schneider, P. D.; Miller, J. D.; Green, R.; Buchholz, B. A.; Vogel, J. S.; Phair, R. D.; Clifford, A. J. *Am. J. Clin. Nutr.* **2004**, *80*, 680–691.

(9) Clifford, A. J.; de Moura, F. F.; Ho, C. C.; Chuang, J. C.; Follett, J.; Fadel, J. G.; Novotny, J. A. *Am. J. Clin. Nutr.* **2006**, *84*, 1430–1441.

(10) Andree, M.; Beer, J.; Oeschger, H. B. G.; Hofmann, H. J.; Morenzoni, E.; Nessi, M.; Suter, M.; Wölfli, W. *Nucl. Instrum. Methods Phys. Res., Sect. B* **1984**, *5*, 274–279.

(11) Vogel, J. S.; Love, A. H. *Methods Enzymol.* **2005**, *402*, 402–422.

(12) Jull, A. J. T.; Donahue, D. J.; Hatheway, A. L.; Linick, T. W.; Toolin, L. J. *Radiocarbon* **1986**, *28*, 191–197.

(13) Kim, S. H.; Kelly, P. B.; Clifford, A. J. *Anal. Chem.* **2008**, *80*, 7651–7660.

* To whom correspondence should be addressed: E-mail: ajclifford@ucdavis.edu. Tel: 530-752-3376. Fax: 530-752-8966.
† Department of Nutrition.
‡ Department of Chemistry.

was to identify the traits of AMS targets that produced intense and reliable ion currents for accurate, precise, reliable, and high throughput for biological/biomedical applications of AMS.

EXPERIMENTAL SECTION

Reagents. The reagents were the same as previously described[7,13] except for the following: Potassium bromide (KBr, CAS No. 7758−02−3, ≥99%, FT-IR grade) and graphite standard (GST, CAS No. 7782−42−5, <20 μm, synthetic powder) were from Sigma-Aldrich (St. Louis, MO).

AMS Target Preparation. AMS targets were prepared by our previous method[7] as well as by our optimized method[13] for which we built a new heating block with 7 rows, 14 holes apiece, to perform at 525 °C ± 0.3 (hole to hole).[13]

AMS Target Characterization. AMS target color values were measured using a Minolta Color meter (Minolta, Ramsey, NJ). The instrument was calibrated against white reflector plate (reference calibrator). The color values represented as $L^{\star}$, $a^{\star}$, and $b^{\star}$ color values. The $L^{\star}$ defines the lightness, and $a^{\star}$ and $b^{\star}$ define red-greenness and blue-yellowness, respectively.[14] Only the lightness values were relevant to the present application.

The hardness of the AMS targets was examined by the TA-XT plus Texture Analyzer (Texture Technologies Corp., Menlo Park, CA). The hardness was expressed as a maximum force (lb) to crush the carbon materials.[15]

The morphological investigation by SEM was the same as previously described.[13]

The FT-IR transmission measurements were performed on the AMS targets using a Nicolet 6700 FT-IR spectrometer (Thermo Scientific, Inc., Waltham, MA) at 23 °C over the range of 4000−400 cm^{-1}, spectral conditions were 4-cm^{-1} resolution and 64 scans. Before FT-IR analyses, ∼3-mg aliquots of AMS targets were ground for ∼2 min with 150 mg of KBr (that had been stored in a desiccator). The KBr and −400MSIP were precalibrated before each measurement.

Raman spectra were performed using a Renishaw microspectrometer (Renishaw Inc. Hoffman Estates, IL) in the continuous scanning mode in the range of 40−4000 cm^{-1}. The 514.5-nm excitation of an Ar ion laser with 5-mW power was introduced with an objective lens (×50 magnification). The 514.5-nm excitation of the Ar ion laser was more sensitive to first- and second-Raman spectra of various graphitic materials than the 632.8 nm of a He−Ne laser or the 780 nm of a NIR diode laser.[16] The laser was focused to a 15−25-μm diameter at the AMS target surface. Peak positions and integral intensities of Raman bands were determined using the SpectraMax microplate spectrophotometer, MaxLine application Note 32 (Molecular Devices Sunnyvale, CA).

The XRD analyses were conducted using the Scintag XDS 2000 (Scintag Inc., Cupertino, CA). The X-ray radiation was from Cu Kα (λ = 0.15418 nm) with an accelerating voltage of 45 kV and a current of 40 mA. A computer-controlled diffractometer collected crystal data in the range (2Θ) of 5°−70° at a speed of 5°/min. The interplane distance d was determined using the Wulff-Bragg

formula,[17] $\lambda = 2d \sin\Theta$ where λ is the wavelength of the X-ray characteristic radiation, d is the basal plane interlayer spacing, and Θ is the diffraction angle. The average crystal size was calculated using the Scherrer equation,[18] $t = K\lambda/(B \cos\Theta)$, where t is the averaged dimension of crystallites (or Lc, stacking height of crystallite to c-direction), K is the Scherrer constant whose value is ∼0.9 (a somewhat arbitrary value in the range 0.87−1.0), λ is the wavelength of X-ray radiation, and B is the half-height width of the diffraction intensity distribution (measured in radians).

RESULTS

Figure 1 is a carbon classification by which AMS targets could be characterized in a relative way. The classification enabled us to rank the degree of crystal (high to low) as graphite crystal > t-C > g-C > i-C, the i-C is highly disordered and approximates amorphous carbon (a-C). The isotropic carbon (i-C), graphitizable semiorder carbon (g-C), turbostratic carbon (t-C), and graphite panels were from a previous publication,[1] with permission.

Figure 2 summarized an overview of the second step of AMS target preparation using our previous[7] and optimized[13] methods. The left panel shows the setup and appearance of the −400MSIP and Zn dust before the reduction. The center and right panels show what happened to the −400MSIP and Zn dust during the reduction using our previous[7] and optimized[13] methods, respectively. Prior to the CO_2 reduction step, the Zn dust and the −400MSIP consisted of loose spherical particles (left panel). After reduction by our previous method[7] (center panel), the Zn dust appeared as a fibrous (rubbery) Zn band-1 at 260 °C, a plasticized or plastic-like Zn band-2 at 380 °C, and two Zn mirrors (mirror 1 at 480 °C and mirror 2 at 525 °C), which appeared to be metallic Zn on the inner wall of the septa-sealed vial. Furthermore, the remaining Zn dust appeared as a Zn cake stuck to the bottom of the septa-sealed vial. Finally, the AMS targets appeared at 540 °C as a graphite-coated iron (GCI) fuzz or a featureless ICM on the −400MSIP at the bottom of the borosilicate inner vial. After reduction by our optimized method,[13] the Zn dust was deformed and appeared as a thinner (compressed) and more fibrous Zn band at 240 °C, a Zn mirror at 380 °C, and a softer Zn cake with less sinter at 500 °C that stuck to the bottom of the septa-sealed vial. The AMS targets appeared as a graphite-coated Fe powder (GCIP) fuzz on the −400MSIP at the bottom of the borosilicate inner vial at 500 °C.

Table 1 summarized the physical and morphological characteristics of the GST as purchased from Sigma-Aldrich and −400MSIP as purchased from Sigma-Aldrich. It also summarized the physical and morphological characteristics of AMS targets of iron-carbon materials (ICM) (produced 20% of the time) and GCI (produced 80% of the time) by our previous method[7] and of GCIP (produced 100% of the time) by our optimized method.[13] The materials were ranked by the lightness of their color as −400MSIP > ICM > GST = GCI = GCIP. The ICM was four times harder than the GCI (p < 0.0001); hardness of powders was not measurable. The photos showed that only the GST, −400MSIP, and GCIP were powders. In comparing SEM of GST to that of −400MSIP, GST was graphite sheets, while −400MSIP was

(14) Gil, M. I.; Holcroft, D. M.; Kader, A. A. *J. Agric. Food Chem.* **1997**, *45*, 1662–1667.
(15) Mitcham, B.; Cantwell, M.; Kader, A. A. *Perishables Handling Newsl.* **1996**, *85*, 1–5.
(16) Sadezky, A.; Muckenhuber, H.; Grothe, H.; Niessner, R.; Pöschl, U. *Carbon* **2005**, *43*, 1731–1742.

(17) Stanjek, H.; Häusler, W. *Hyperfine Interact.* **2004**, *154*, 107–119.
(18) Cullity, B. D. *Elements of X-ray Diffraction,* 2nd ed.; Addison Wesley: Reading, MA, 1978.
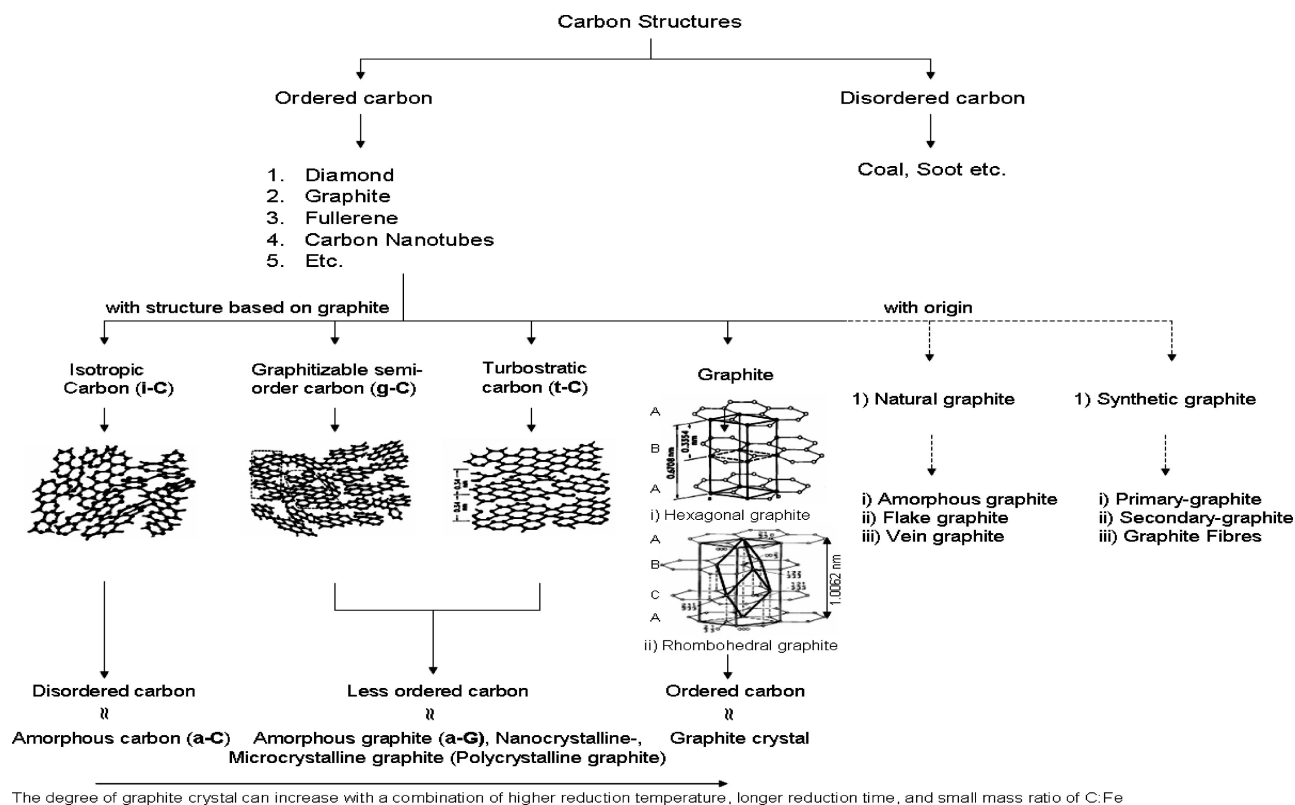
Figure 1. Schematic of carbon classification based on graphite. The classification enabled the degree of crystal to be ranked (high to low) as graphite crystal > t-C > g-C > i-C. The i-C is highly disordered and approximates amorphous carbon (a-C). The isotropic carbon (i-C), graphitizable semiorder carbon (g-C), turbostratic carbon (t-C), and graphite panels were from a previous publication.[1] Rhombohedral graphite panel was from http://www.bas.bg/cleps/events/see/Presentations/SED_07_Trifonova.pdf.
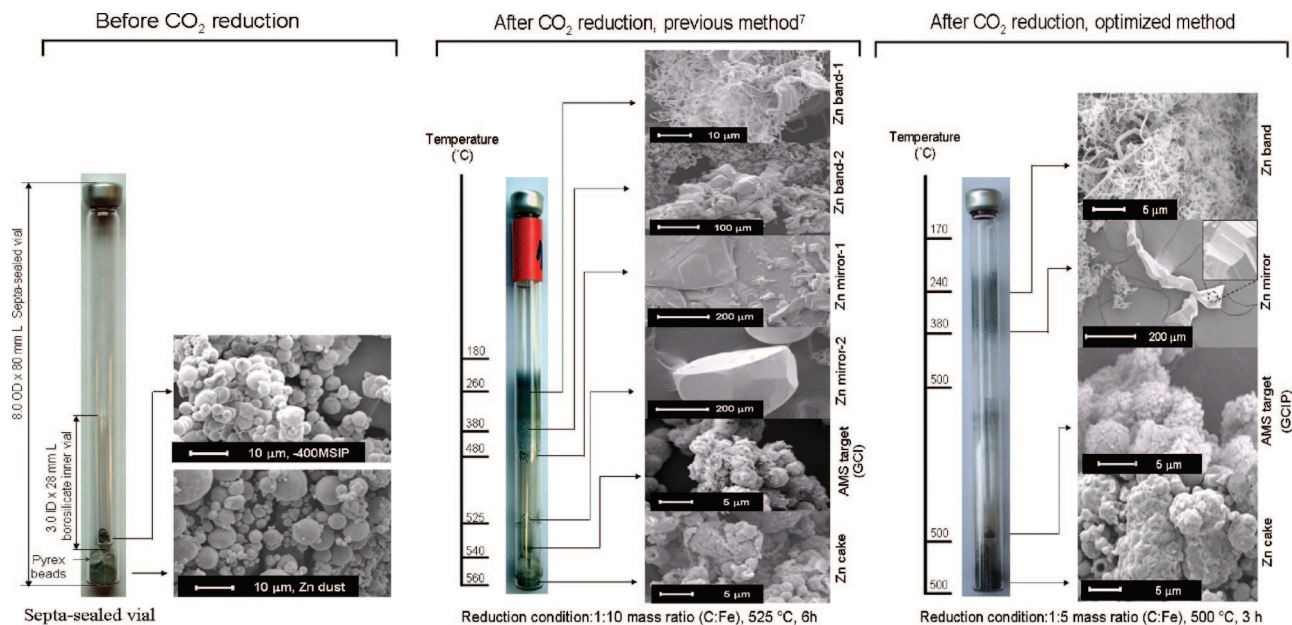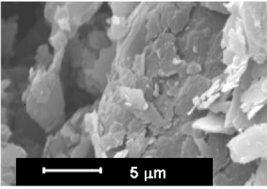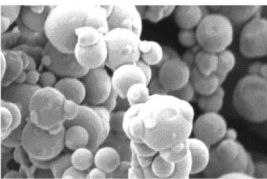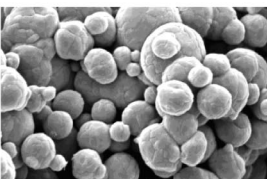

Figure 2. Summary of the temperature gradient along the septa-sealed vial using our previous[7] (center panel) and our optimized[13] (right panel) methods. It also shows SEMs of the Zn deposits along the septa-sealed vials and of the AMS targets (GCI, GCIP) in the borosilicate inner vials. Our previous method produced AMS targets of gray-colored ICM 20% of 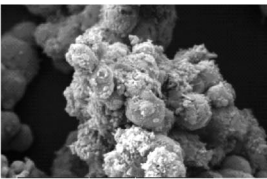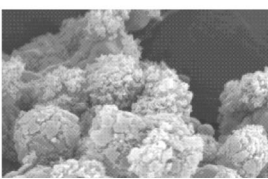the time and of GCI 80% of the time; neither target was a powder. Our optimized method[13] produced AMS targets of 100% GCIP 100% of the time.[13] AMS targets of GCIP produced more intense and reliable ion currents and more accurate F_m values than those of ICM or GCI. The left and center panels were from ref 13. The SEM picture (third from top, GCIP) in the right panel was also from ref 13.

spherical, and the particle size of each was ≤37 μm. The SEMs also showed the surface of ICM as featureless, of GCIP as uniform fuzz, and of GCI as nonuniform fuzz. Even though the SEMs alone did not distinguish between Fe_3C crystal, i-C, g-C, t-C, and graphite

Table 1. Physical and Morphological Characteristics of Graphite Standard (GST), and of −400 Mesh Spherical Fe Powder (−400MSIP)[a]

	Color, Lightness	Hardness, lb	Photo	SEM
Color calibrator	97.2	-		
Graphite Standard (GST, < 20 μm, synthetic, CAS #7782-42-5, Sigma-Aldrich)	31.6 ± 0.1 [a] (n=3)	-		
-400 mesh spherical Fe powder (-400MSIP, 99.99+ %, CAS # 7439-89-6, Sigma-Aldrich)	44.1 ± 0.6 [c] (n=3)	-		
Iron-carbon materials (ICM) produced during the CO_2 reduction step by our previous method (10 mg Fe powder and 525 °C for 6 h).	39.7 ± 0.8 [b] (n=15)	8.4 ± 0.9 [a] (n=10)		
Graphite-coated Fe (GCI) produced during the CO_2 reduction step by our previous method (10 mg Fe powder and 525 °C for 6 h).	30.8 ± 0.3 [a] (n=15)	2.0 ± 0.4 [b] (n=10)		
Graphite-coated Fe (GCIP) produced during the CO_2 reduction step by our optimized method[13] (5 g Fe powder and 500 °C for 3 h).	31.2 ± 0.4 [a] (n=15)	-		

[a] Also shown are the physical and morphological characteristics of ICM and GCI by our previous method[7] and of GCIP by our optimized method.[13] The SEM pictures (2nd, −400MSIP; 4th, GCI; 5th, GCIP from top) were from ref 13.

crystal, the carbon classification in Figure 1, enabled the degree of crystal to be ranked (high to low) as graphite crystal > t-C > g-C > i-C. The i-C is highly disordered and approximates a-C. Finally, the GCIP was the most facile to tamp into the AMS target holder.

Figure 3 showed FT-IR transmission spectra of GST and of the AMS targets ICM, GCI, and GCIP, all showed a water band at ∼1630 cm^{-1}, and except for ICM, and all showed a band at ∼1580 cm^{-1} that corresponded to the sp^2 bond (C=C bond stretching) in graphite. The band at ∼1580 cm^{-1} indicated that GCI and GCIP each had a carbon hexagonal structure.

Figure 4 summarized the Raman spectra of GST, ICM, GCI, and GCIP (left panel) in relation to Raman spectra from the scientific literature (right panel) with permission. The D, G, and G′ (G′ = 2D = D*) bands correspond to the sp^3 bond (diamond-like carbon), sp^2 bond (graphite and graphite-like carbon), and stacking arrangement without disorder (graphite crystal), respectively. The GST showed intense G and G′ bands at 1566.3 and 2705.4 cm^{-1} and weak D and D″ bands at 1339.0 and 3228.5 cm^{-1}, respectively. The ICM appeared to have only weak D and G bands

at 1329.4 and 1584.7 cm^{-1} and no evidence of G′ or a G + D combination band that would indicate second-order Raman scattering. The GCI showed intense D and G bands at 1321.5 and 1585.7 cm^{-1}, respectively. In addition, GCI showed G′, G + D combination, and D″ bands at 2655.7, 2917.2, and 3203.6 cm^{-1} respectively. The Raman spectrum of GCIP was similar to that of GCI, and it also showed the first-order (D and G bands) and second-order Raman scattering (G′, G + D, and D″ bands). The full width at half-maximum height (fwhm, Δ) of D, G, and G′ bands in GST was narrow, while the fwhm of those same bands in ICM, GCI, and GCIP were two to three times broader than those same corresponding bands in GST. The in-plane crystallite size (L_a) was inversely proportional to the I_D/I_G, and GST > GCI > ICM = GCIP were ranked large to small based on their L_a.

Figure 5, panel A showed the XRD spectra of GST and −400MSIP. The GST had an intense diagnostic graphite-002 reflection peak (G-002) at ∼26.5°; its intensity was 5−33 times greater than that of G-004, G-100, or G-101 peaks. Thirty milligrams of GST had a stacking height of crystal (often called L_c) of 15.42 nm and an interlayer distance (d) of 0.334 nm. The
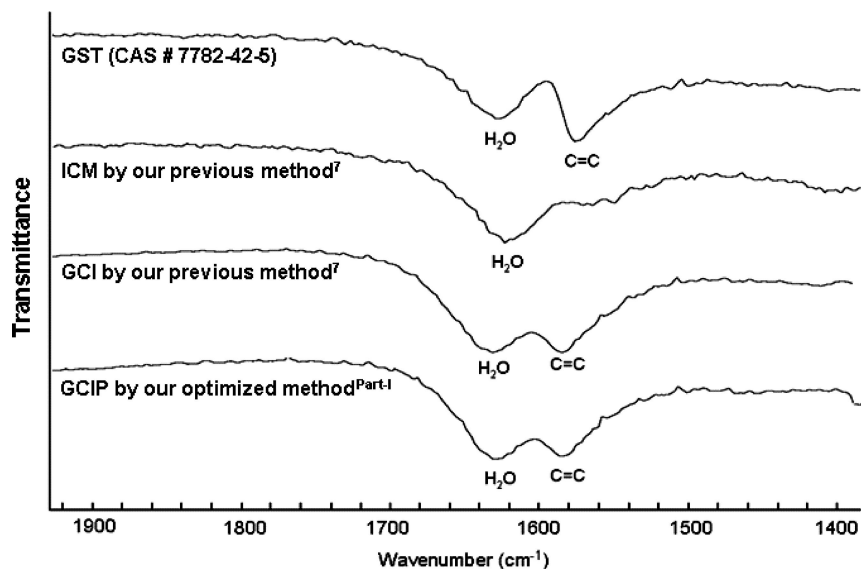
Figure 3. FT-IR transmission spectra of GST, ICM, GCI, and GCIP. All spectra showed a water band at $\sim 1630 \text{ cm}^{-1}$. All spectra, except that of ICM, showed a band at $\sim 1580 \text{ cm}^{-1}$. This band corresponded to the sp^2 bond (C=C bond stretching) in graphite, and it demonstrated that GCI and GCIP each consisted of a carbon hexagonal structure.

-400MSIP, often called α-Fe or body-centered cubic lattice iron (bcc-Fe), had the α-Fe (110) reflection peak at $\sim 45°$ and the α-Fe (200) reflection peak at $\sim 65°$. Forty milligrams of α-Fe had a L_c of 29.11 nm and an interlayer distance of 0.202 nm using α-Fe-110 as reference.

Figure 5, panel B summarized XRD spectra of the AMS targets ICM, GCI, and GCIP. Consistent with prior studies,[19−21] there was no evidence of a G-002 peak at $\sim 26.5°$ in ICM, GCI, or GCIP, detecting only Fe_3C crystal with possible traces of Fe_xC_y and α-Fe crystals within the range of $30°−70°$ (2Θ).

Even if GCI spectrum lacked a G-002 peak, it still suggested the presence of g-C because FT-IR and Raman spectra of GCI showed a mix with some sp^2 and sp^3 carbon bond structures. As already seen from Figure 1, the i-C and g-C have an "amorphous (disordered)" and an "less ordered" carbon structure, respectively. The XRD spectrum of GCIP was very similar to those of ICM and GCI, and when the FT-IR and Raman spectra were considered together, the GCIP consisted of g-C and Fe_3C crystal. The G-101 refection peak overlapped that of Fe_3C and of α-Fe (110), so it was difficult to individually differentiate graphite from α-Fe and Fe_3C at $\sim 45°$.

Figure 5, panel C showed relative sensitivity toward 1:1, 1:10, and 10:1 ratios of GST/GCIP (including Fe_3C and α-Fe crystals) to Cu Kα, the X-ray source. A good quality XRD spectrum of graphite crystal (especially, G-002) required an AMS target that contained ≤ 2 mg of graphite crystal. In all ratios of GST/GCIP, the G-002 reflection peak was much more sensitive than the reflection peaks of Fe_3C or α-Fe crystals. Finally, the graphite crystal mass of ICM, GCI, and GCIP was ≤ 2 mg. The absence of a G-002 reflection peak indicated that ICM, GCI, and GCIP each consisted of a mix of Fe_3C crystal and g-C rather than of a graphite

crystal. The ICM had more iron carbide (Fe_3C) crystal than g-C, and ICM produced low and variable ion current whereas the opposite was true for GCI and especially so for GCIP.

DISCUSSION

A variety of graphite-like substances are formed during the reduction of CO_2 to AMS targets depending on the conditions used. The types of graphite-like substances include filamentous,[4] fluffy, and firm or solid graphite;[22] these substances differ from one another in a variety of traits such as color, hardness, texture, SEM, FT-IR, Raman, and XRD spectra. To the extent that the traits affect the magnitude of the ion current produced, they are important so, we determined these traits in AMS targets produced using our previous[7] and optimized methods.[13] Our goal was to identify those traits in AMS targets that produced intense and reliable io1n currents for accurate, precise, reliable, and high-throughput measurements of ^{14}C using AMS.

Our previous method formed GCI (black, soft pellet, less uniform, fuzz) 80% of the time and ICM (gray, hard pellet, featureless carbon deposition) 20% of the time.[7] On the other hand our optimized CO_2 reduction method formed only GCIP (black, soft powder, uniform, fuzz) 100% of the time.[13] In general, the presence of a nongraphitic carbon or Fe_3C crystal resulted in the formation of a harder carbon structure than a compact graphitized carbon.[23,24]

Graphite produced ion currents of 13.4 μA of $^{12}C^{4+}$/mg of C while a-C produced ion currents that ranged from 5.4 to 7.4 μA of $^{12}C^{4+}$/mg of C.[3] Furthermore, the presence of cobalt carbide in AMS targets produced still lower ion currents whose associated error in the $^{14}C/^{13}C$ ratio was as high as 10%.[5] Because the ion current produced by ICM was 13% lower than that produced by

(19) Jaer, C.; Mutschke, H.; Huisken, F.; Alexandrescu, R.; Morjan, I.; Dumitrache, F.; Barjega, R.; Soare, I.; David, B.; Schneeweiss, O. *Appl. Phys., A: Mater. Sci. Process.* **2006**, *85*, 53–62.

(20) Nikitenko, S. I.; Koltypin, Y.; Palchik, O.; Felner, I.; Xu, X. N.; Gedanken, A. *Angew. Chem., Int. Ed.* **2001**, *40*, 4447–4449.

(21) Chung, U. C.; Kim, Y. H.; Lee, D. B.; Jeong, Y. U.; Chung, W. S.; Cho, Y. R.; Park, I. M. *Bull. Korean Chem. Soc.* **2005**, *26*, 103–106.

(22) Santos, G. M.; Mazon, M.; Southon, J. R.; Rifai, S.; Moore, R. *Nucl. Instrum. Methods Phys. Res., Sect. B* **2007**, *259*, 308–315.

(23) Franklin, R. E. *Proc. R. Soc. London., Ser. A: Math. Phys. Sci.* **1951**, *209*, 196–218.

(24) Wagner, D. B. *Iron and Steel in Ancient China*; E.J. Brill: London, 1993; pp 335–344..
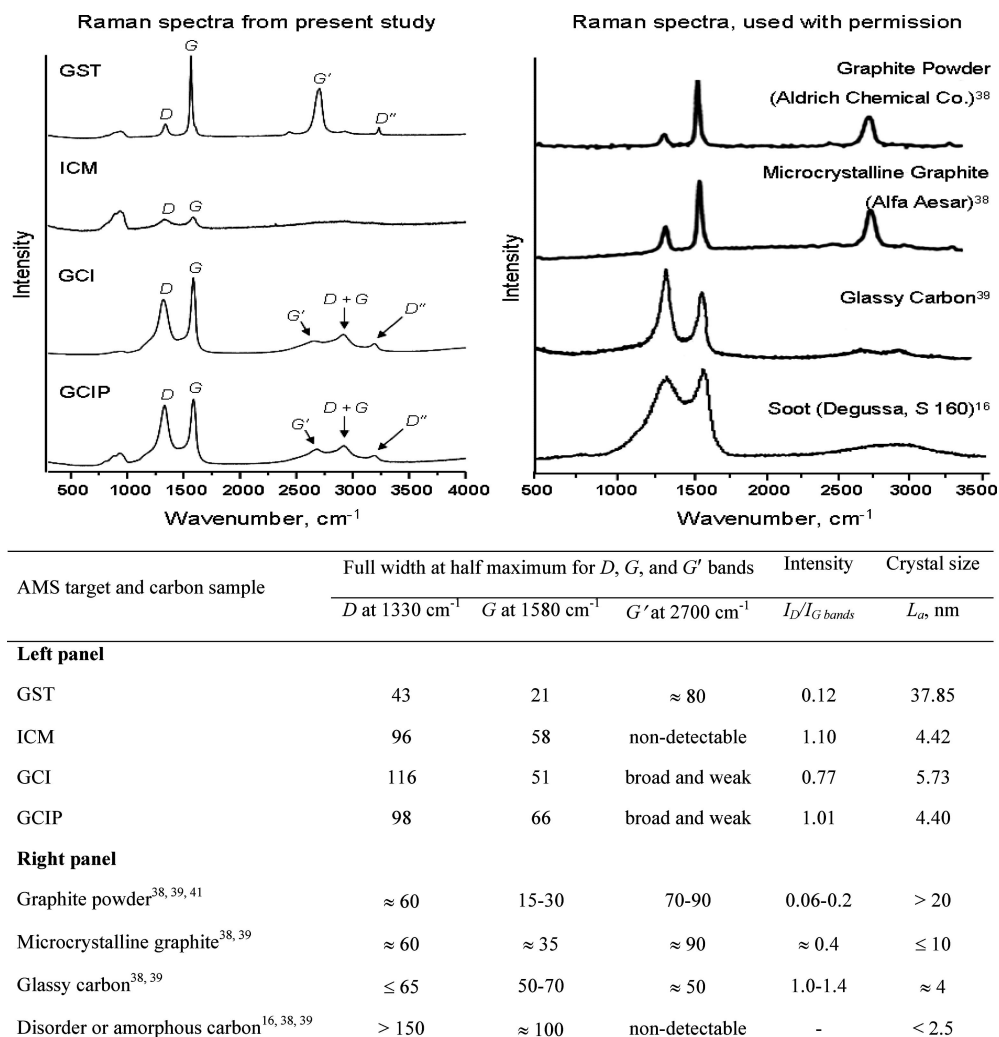
Figure 4. Raman spectra of GST, ICM, GCI, and GCIP compared to published spectra of similar materials. Crystal size, in-plane, of graphite (L_a) = $C/(I_D/I_G)$, where $C \approx 4.4$ nm. Intensities of the G′ of commercially available glassy carbon are variable and are classified as narrow and strong or nondetectable.[38,39] Soot is a highly disordered graphitic structure or amorphous carbon, because it consists of graphite-like crystalline and amorphous carbon domains. So, intensities of the D, G, G′, D+G, and D″ bands from commercially available soot depend on the completeness solid carbon conversion to CO_2 and on the degree to which CO_2 is converted to graphite.[16]

AMS target and carbon sample	Full width at half maximum for D, G, and G' bands			Intensity	Crystal size
	D at 1330 cm^{-1}	G at 1580 cm^{-1}	G' at 2700 cm^{-1}	$I_D/I_{G\ bands}$	L_a, nm
Left panel					
GST	43	21	≈ 80	0.12	37.85
ICM	96	58	non-detectable	1.10	4.42
GCI	116	51	broad and weak	0.77	5.73
GCIP	98	66	broad and weak	1.01	4.40
Right panel					
Graphite powder[38,39,41]	≈ 60	15-30	70-90	0.06-0.2	> 20
Microcrystalline graphite[38,39]	≈ 60	≈ 35	≈ 90	≈ 0.4	≤ 10
Glassy carbon[38,39]	≤ 65	50-70	≈ 50	1.0-1.4	≈ 4
Disorder or amorphous carbon[16,38,39]	> 150	≈ 100	non-detectable	-	< 2.5

GCI and by GCIP, isotopic fractionation occurred in ICM. In addition, the F_m values of ICM (1.3355) were ~0.4% lower than those of Ox-2 SRM (1.3407), GCI (1.3429), and GCIP (1.3410), confirming prior reports.[3,5] Furthermore, a large ratio of Fe/C (15:1) favored ICM formation,[4,25] so by reducing the Fe/C ratio from 10:1 to 5:1, the formation of ICM was completely avoided.[13] We did not find FT-IR, Raman, or XRD spectra of AMS targets in our search of the literature, so assumed that the ICM was mostly Fe₃C and some i-C or g-C rather than single graphite crystal. This observation prompted us to further investigate characteristics of AMS targets with FT-IR, Raman, and XRD.

FT-IR and Raman Spectroscopy. FT-IR enabled the vibration of aromatic structures in graphite to be investigated. For FT-IR, the KBr pellet showed a good spectrum by transmission measurements for the aromatic structure of graphite, because FT-IR spectra are not associated with crystal structure of graphite.[26] The KBr pellet produced a band ~1630 cm^{-1} (H_2O molecule) due to a moisture effect, and it was partially overlapped with the ~1580 cm^{-1} of the graphite band.[24] The FT-IR spectra of GCI and GCIP were consistent with that of GST in Figure 3 and with those in previous reports.[26,27]

As shown in Figure 3, the bands at ~1580 cm^{-1} for GCI and GCIP were less well resolved than the corresponding band for GST. The poor resolution suggested that GCI and GCIP might consist of i-C, g-C, or t-C; the GCI and GCIP had the appearance of disordered graphite or less ordered graphite compared to ordered graphite crystal. The FT-IR spectra of graphite showed its strong and characteristic band (~1580 cm^{-1}) that has been attributed to lattice vibration or "aromaticity" of the graphite and it can be identified with acoustic E_{1u} mode including $\hat{E}_{1u}$, E^*_{1u}, and E^o_{1u}.[26-29] The weak band of graphite, sometimes measured at 830 cm^{-1}, was due to an aromatic impurity such as oxygen or nitrogen in graphite. Also, a-C showed two broad bands, one at

(25) Dee, M.; Ramsey, C. B. *Nucl. Instrum. Methods Phys. Res., Sect. B* **2000**, *172*, 449–453.

(26) Friedel, R. A.; Carlson, G. L. *J. Phys. Chem.* **1971**, *75*, 1149–1151.

(27) Smith, D. M.; Griffin, J. J.; Goldberg, E. D. *Anal. Chem.* **1975**, *47*, 233–238.

(28) Tuinstra, F.; Koenig, J. L. *J. Chem. Phys.* **1970**, *53*, 1126–1130.

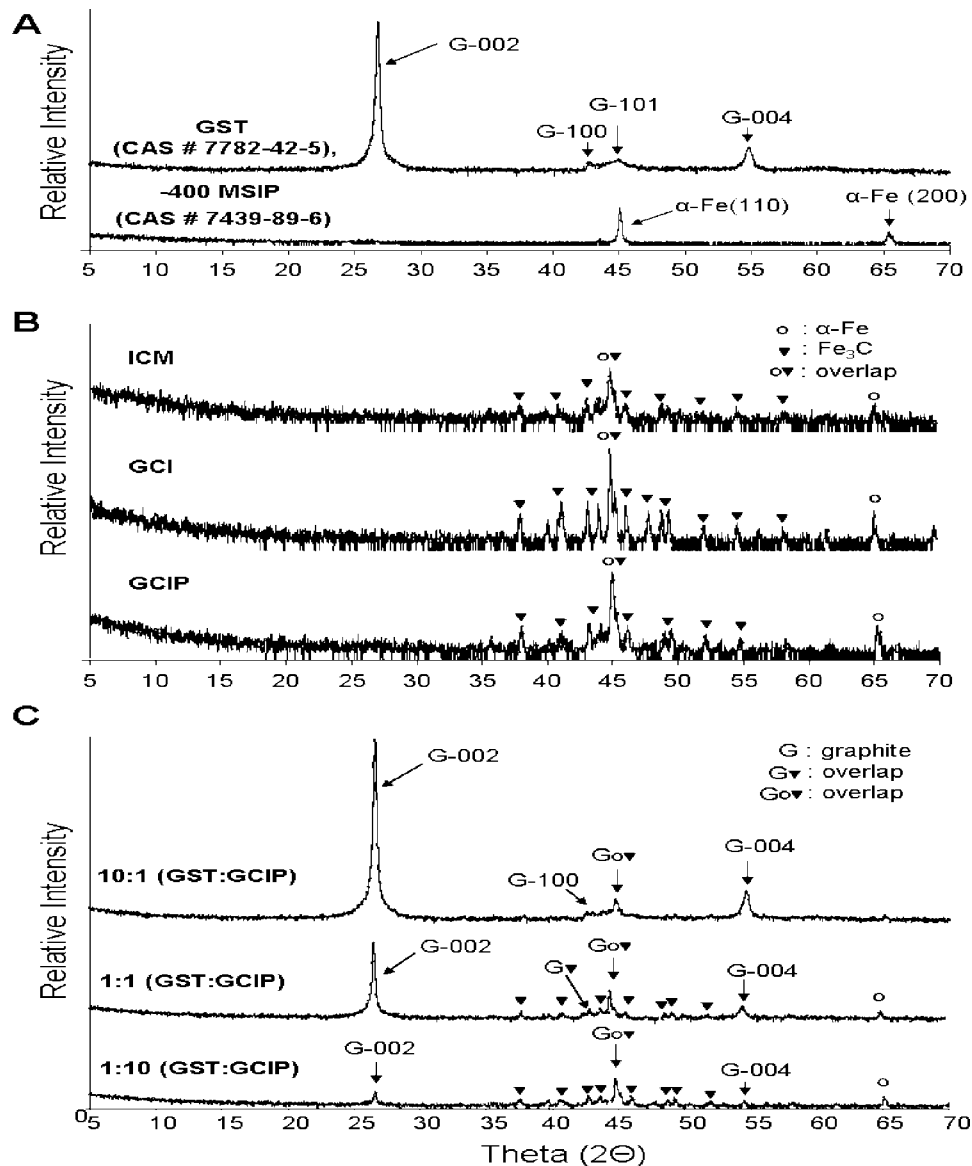(29) Gualberto, G. M.; Underhill, C.; Leung, S. Y.; Dresselhaus, G. *Phy. Rev. B* **1980**, *21*, 862–868.

Figure 5. XRD spectra of GST, −400MSIP (reference standards, panel A), ICM, and GCI, using our previous method and GCIP using our optimized method[13] (panel B), and 10:1 to 1:10 mixes of GST/GCIP (panel C). In panel A, GST had a G-002 reflection at ~26.5° while −400MSIP had α-Fe-110 and α-Fe-200 reflections at ~45° and ~65°, respectively. Also, the G-002 reflection was more sensitive than either the α-Fe or Fe$_3$C crystal reflections. In panel B, ICM, GCI, and GCIP spectra had no (<2 mg of graphite crystal) detectable G-002 reflection, but they did have detectable Fe$_3$C crystal and α-Fe crystal reflections at 35°−70°. Absence of a G-002 reflection indicated that ICM, GCI, and GCIP each consisted of a mix of Fe$_3$C crystal, i-C, and g-C rather than being a single graphite crystal. In panel C, the sum of GST+GCIP in the mix was 22 mg. In all ratios of GST/GCIP, the G-002 reflection was more sensitive than that of Fe$_3$C or α-Fe crystals. Also, the graphite crystal mass of ICM, GCI, and GCIP was ≤2 mg. The ICM was mostly Fe$_3$C crystal and the ICM contained less than half as much g-C compared to GCI and GCIP.

~1350 cm^{-1} and the other at ~1580 cm^{-1}. The band at ~1350 cm^{-1} often combined with the band at 830 cm^{-1} to appear as a weak band at ~2200 cm^{-1}. Therefore, FT-IR spectra of graphite (devoid of a-C and of aromatic impurity) would be devoid of the 830-, ~1350-, and ~2200-cm^{-1} bands.[26,27]

The Raman spectroscopy is more useful than FT-IR to determine the presence and features of graphite and disordered carbon, yet we found no information on iron carbide using the Raman in literature.[30] The main features of graphitic materials in the Raman spectra were called G (~1560 cm^{-1}, E$_{2g}$ mode, sp^2) and D (~1360 cm^{-1}, A$_{1g}$ mode, sp^3) bands for visible excitation,

while the a-C band (T band) appears at ~1060 cm^{-1} seen in UV excitation.[26,29,31,32] The iron carbide band was expected to appear between 200 and 600 cm^{-1} by Raman, but it was not detected because the low-energy vibration frequencies are too close to the laser line to be detected.[33] The D band was first reported as a disorder-induced mode.[28] The sp^3 carbon bond content (D band) increased as amorphization and micro- and nanocrystalline graphitic materials were observed.[34] The origin of the D band at 1350

(30) Park, E. Y.; Zhang, J. Q.; Thomson, S.; Ostrovski, O.; Howe, R. *Metall. Mater. Trans. B* **2001**, *32B*, 839–845.

(31) Merhari, L.; Belorgeot, C.; Quintard, P. *J. Mater. Sci. Lett.* **1994**, *13*, 286–288.

(32) Ferrari, A. C.; Robertson, J. *Phys. Rev. B* **2001**, *64*, 075414. 13 pages.

(33) Bi, X. X.; Ganguly, B.; Huffman, G. P.; Huggins, F. E.; Endo, M.; Eklund, P. C. *J. Mater. Res.* **1993**, *8*, 1666–1674.

cm^{-1} is an unsettled issue. In practice, because a perfect single graphite crystal is hardly ever obtained with high temperature, all graphite materials have defects of different types. Heat treatment of graphite materials can reduce the intensity of the D band at 1350 cm^{-1}, however, the D band is still present even at 3000 °C.[35,36] Therefore, a perfect graphite crystal did not show D, D′, or D + G bands because they are defect-induced Raman features.[35] In disordered, microcrystalline, and nanocrystalline graphite, the D′ band at 1620 cm^{-1} merged with the G band, and the intensity of the merged bands increased with edge carbon atoms or as the relative content of disordered carbon increased. Also, the D″ band was inaccurately assigned as a defect-induced feature (artifact).[37] Finally, disorder in the graphite structure modified the C−C bond vibrations, and therefore broadened (increased fwfm) the D and G bands.[36−38] The crystal size in graphitic materials was inversely related to the fwhm of D and G bands because the fwhm of D and G bands included defects in graphitic materials. The disordered graphitic materials showed a broader D band (>150 cm^{-1}) than ordered graphitic materials (~60 cm^{-1}). In addition, the G′ band corresponded to overtone of the D band, and the ratio of I_D/I_G (not $I_{D'}/I_G$) was inversely related to L_a. The L_a can be determined to be ~2 nm using the TK formula, and it underestimated L_a due to the domain effect of small crystal compared to XRD measurement.[34−41]

As a result, ICM was mostly iron carbide (Fe_3C, cementite) with only traces of nanocrystalline graphite or disordered graphite because iron carbide-like Fe_3C formation precedes graphite structure formation.[42] The D, G, D′, and D + G bands of GCI and GCIP were consistent with prior reports.[30,35,36] Therefore, the GCI and GCIP were less-ordered graphitic materials rather than single graphite crystal mixed with Fe_3C crystal, nanocrystalline graphite, or sp^3 carbon structure (D band) that were placed mostly in the edge of GCI and GCIP.

Although the formation of graphite and its crystal size increased at higher CO_2 reduction temperatures, the difference in L_a between GCI and ICM formed at 559 ± 7 °C for 6 h compared to GCIP formed at 500 ± 0.3 °C for 3 h was not significant statistically. However, the higher CO_2 reduction temperature (>585 °C) can produce more ordered graphite crystal without disordered structure. Because our FT-IR and Raman results suggested that ICM, GCI, and GCIP consisted of a mix of nanocrystalline graphite (or g-C), and Fe_3C crystal, we further examined the AMS targets using XRD to distinguish between crystal and amorphous structures.

XRD. Graphite crystal is found in two forms: hexagonal graphite that has the stacking sequence ABAB and rhomboheral graphite that has the layer sequence ABCABC (Figure 1). The natural abundance of graphite type is 70% hexagonal and 30% rhombohedral.[2] The unit cell of graphite has dimensions a, b, and c along x, y, and z axes and also an interlayer distance, d. For graphite, $a = b$ ~0.246 nm, c ~0.670, and d ~0.334 nm.[17] The degree of graphite crystal is diminished as the d values increase.[12] The graphite crystal is generally formed at temperatures ≥2000 °C, whereas at 400−1000 °C, the carbon formed a disordered (or less-ordered) structure-like i-C or g-C.[1,19,43]

Most graphitization methods for AMS targets reduced CO_2 to "graphite",[3−5] a fullerene "graphite",[6] or "solid fullerene"[11] and sometimes to a MeC, such as cobalt or iron carbide.[5,12] Both H_2 and Zn (dust) are each commonly used as a reductant. The Zn reduction method produced graphite crystal with a consistent line broadening (0.55°−0.65°) for the G-002 reflection peak with some less crystallized material.[12]

In the beginning, we expected that GCI and GCIP to be graphite crystal (or t-C) and ICM to be mostly Fe_3C crystal. However, we did not find pure graphite crystal in either GCI or GCIP. If GCI and GCIP contained pure graphite crystal, it would show an intense and sharp G-002 reflection peak at ~26.5°. Furthermore, if GCI and GCIP were t-C, they should also show a little broad G-002 reflection peak at ~26.5° depending on the degree of the defect of graphite crystal. However, the GCI and GCIP may be nanocrystalline graphite that lacked a stacking arrangement, because detecting graphite crystal <20 nm in size using XRD is not practical.[35] Based on the absence of C=C stretching in FT-IR spectra, weak D and G bands in Raman spectra, and a clear presence of Fe_3C crystal in XRD spectra, we concluded that the ICM was mostly Fe_3C crystal with a minimal amount of sp^2 (g-C including nanocrystalline graphite) and sp^3 (edge-carbon in graphite). The GCI and GCIP were also a mix of nanocrystalline graphite (or g-C) and Fe_3C crystal based on FT-IR (C=C), Raman spectra (D, G, G′, and D + G bands), and XRD (Fe_3C crystal). The g-C and Fe_3C crystal was were preferentially formed over single graphite crystal by our previous[7] and our optimized[13] methods, formation of perfect graphite crystal might be possible with a combination of higher CO_2 reduction temperature and smaller mass ratio of C/Fe. Longer reduction time combined with higher CO_2 reduction temperature and smaller mass ratio of C/Fe may be useful to also minimize defects of in the graphite crystal.

As soon as AMS targets were produced, an overnight cooldown to room temperature (similar to annealing process) did not produce well-ordered larger graphite crystal compared to a 3-min cooldown. The graphitization yield and isotopic fragmentation were not influenced by the duration of a slow cooldown. Ion currents were affected more by the amount of graphite rather than its crystal size. Consequently a 3-min cooldown facilitated a high throughput for biological/biomedical applications of AMS. Previously a skilled analyst could prepare 60−150 AMS targets per day,[5−7] while our optimized method produced as many as 270 AMS targets per d/skilled analyst.

CONCLUSIONS

AMS targets of GCI and GCIP each produced a mix of nanocrystalline graphite (or g-C), and Fe_3C crystal, intense $^{12}C^-$

(34) Ferrari, A. C.; Robertson, J. *Physc. Rev. B* **2000**, *61*, 14095–14107.

(35) Pimenta, M. A.; Dresselhaus, G.; Dresselhaus, M. S.; Cançado, L. G.; Jorio, A.; Saito, R. *Phys. Chem. Chem. Phys.* **2007**, *9*, 1276–1291.

(36) Hirlimann, C.; Jouanne, M.; Forrières, C. *J. Raman Spectrosc.* **1992**, *23*, 315–317.

(37) Reigh, S.; Thomsen, C. *Phil. Trans. R. Soc., London A* **2004**, *362*, 2271–2288.

(38) Escribano, R.; Sloan, J. J.; Siddique, N.; Sze, N.; Dudev, T. *Vib. Spectrosc.* **2001**, *26*, 179–186.

(39) Knight, D. S.; White, W. B. *J. Mater. Sci.* **1989**, *4*, 385–393.

(40) Nakamura, K.; Fujitsuka, M.; Kitajima, M. *Phys. Rev. B* **1990**, *41*, 12261–12263.

(41) Nikiel, L.; Jagodzinski, P. W. *Carbon* **1993**, *31*, 1313–1317.

(42) Santos, G. M.; Southon, J. R.; Griffin, S.; Beaupre, S. R.; Druffel, E. R. M. *Nucl. Instrum. Methods Phys. Res., Sect. B* **2007**, *259*, 293–302.

(43) Onodera, A.; Higashi, K.; Irie, Y. *J. Mater. Sci.* **1998**, *23*, 422–428.

current consistently, with only traces of isotopic fragmentation, and accurately estimated the F_m values. The GCIP produced by our optimized method[13] consistently produced ~115 μA of $^{12}C^-$ and accurate and precise F_m value with a throughput of up to 270 AMS targets per skilled analyst/d for biological/biomedical AMS applications.